RSPECT: Robust and Scalable Planner for Energy-Aware Coordination of UAV-UGV Teams in Aerial Monitoring

Cahit Ikbal Era, Amin Kashirib, Yasin Yazıcıoğlua,b,*

^aDepartment of Mechanical and Industrial Engineering, Northeastern University, Boston, MA, 02115, USA ^bDepartment of Electrical and Computer Engineering, Northeastern University, Boston, MA, 02115, USA

Abstract

We consider the robust planning of energy-constrained unmanned aerial vehicles (UAVs) and unmanned ground vehicles (UGVs), which act as mobile charging stations, to perform long-horizon aerial monitoring missions. More specifically, given a set of points to be visited by the UAVs and desired final positions of the UAV-UGV teams, the objective is to find a robust plan (the vehicle trajectories) that can be realized without a major revision in the face of uncertainty (e.g., unknown obstacles/terrain, wind) to complete this mission in minimum time. We provide a formal description of this problem as a mixed-integer program (MIP), which is NP-hard. Since exact solution methods are computationally intractable for such problems, we propose RSPECT, a scalable and efficient heuristic. We provide theoretical results on the complexity of our algorithm and the feasibility and robustness of resulting plans. We also demonstrate the performance of our method via simulations and experiments.

Keywords: Multi-robot systems, unmanned vehicles, aerial monitoring, energy-aware planning, robust planning

We consider the robust planning of energy-constrained unmanner which act as mobile charging stations, to perform long-horizon at to be visited by the UAVs and desired final positions of the UA trajectories) that can be realized without a major revision in the complete this mission in minimum time. We provide a formal desis NP-hard. Since exact solution methods are computationally in efficient heuristic. We provide theoretical results on the complex plans. We also demonstrate the performance of our method via some security. Multi-robot systems, unmanned vehicles, aerial monomorphisms. We also domains such as precision agriculture, logistics, disaster response, security, and environment/infrastructure monitoring (e.g., [1, 2, 3, 4, 5, 6]). One of the main roles of UAVs in such applications is to perform aerial monitoring, i.e., collecting sensor data (e.g., aerial images) from desired locations. In missions defined over large areas or long time-horizons, a major limitation of UAVs is their limited battery capacity. This limitation can be addressed by deploying some charging stations (e.g., [7, 8, 9]). However, this approach requires establishing some infrastructure on the ground, which may be very inefficient or infeasible in some scenarios (e.g., missions over very large areas or in remote locations). Alternatively, the UAVs can be supported with unmanned ground vehicles (UGVs), which serve as mobile charging stations and transport the UAVs between different take-off/landing locations.

Recently, there has been a growing interest in energy-aware planning of UAV-UGV teams. In [10], given a set of points

Recently, there has been a growing interest in energy-aware planning of UAV-UGV teams. In [10], given a set of points to be visited by the UAV, first a set of rendezvous locations (charging stops) are computed based on Voronoi tessellations, then the UAV and UGV trajectories are computed separately via a genetic algorithm and a variant of A^* . In [11], the authors propose an algorithm that determines the UAV path and the optimal locations for landing on stationary or mobile UGV-based charging stations by formulating the problem as a variant of the

kashiri.a@northeastern.edu (Amin Kashiri), y.yazicioglu@northeastern.edu (Yasin Yazıcıoğlu) Generalized Traveling Salesperson Problem (GTSP). In [12], the authors propose a two-stage heuristic for UAV-UGV route planning with energy constraints, leveraging a mobile ground vehicle constrained to a road network as a refueling station to maximize coverage. In [13], the authors present a scalable heuristic for persistent surveillance by partitioning the environ-

ment into smaller regions that can be covered in a single tour by the energy-limited UAVs, which are recharged and transported

between those regions by the UGVs. Most of these studies have focused on planning UAV and UGV paths in the absence of uncertainty (e.g., the map/obstacles are known, no uncertainty in fuel consumption). In [14], the authors use linear programming to find optimal rendezvous points to modify the trajectories of a UGV (charging station) and an energy-limited UAV with stochastic fuel consumption. In [15], the authors build on [13] to achieve scalable and robust planning of UAV-UGV

teams in persistent surveillance problems in the face of a priori unknown obstacles.

In this paper, we propose a scalable and efficient algorithm for robust planning of UAV-UGV teams to perform longhorizon aerial monitoring missions. In particular, we consider missions where a given set of aerial locations must be visited by a collection of UAV-UGV teams, each of which consist of an energy-limited UAV and a supporting mobile charging station (UGV). Each team starts from an initial location and must end the mission at a specified final location. The goal is to achieve robust offline planning of the vehicles to minimize the overall mission completion time while ensuring that all aerial locations will be visited by one of the UAVs without violating the UAVs' energy constraints, even in the face of disturbances that may cause longer travel times or deviations from the offline plan. The main contributions of this paper are as follows:

^{*}Corresponding author.

Email addresses: er.c@northeastern.edu (Cahit Ikbal Er),

- We formulate a novel robust, energy-aware, multi UAV-UGV planning problem as a mixed-integer program.
- 2. We propose a scalable and efficient heuristic, RSPECT (Alg.1), to solve this NP-hard planning problem.
- 3. We present theoretical results on the computational complexity (Theorem 1) and robustness (Theorem 2, Corollary 2) of our algorithm.
- 4. We demonstrate the performance of our approach via simulations, experiments, and numerical comparisons with some standard optimization techniques (branch and cut, simulated annealing, genetic algorithm) and other heuristics proposed in closely related works [10, 11, 12].

2. Problem Formulation

We use \mathbb{R} and $\mathbb{R}_{\geq 0}$ to denote the sets of real numbers and nonnegative real numbers, respectively. We consider an aerial monitoring mission, where small UAVs are supported by UGVs, which serve as mobile charging stations and transport the UAVs between take-off/landing locations. An overview of the representative multi-team UAV–UGV aerial monitoring mission environment considered in this work is illustrated in Fig. 1

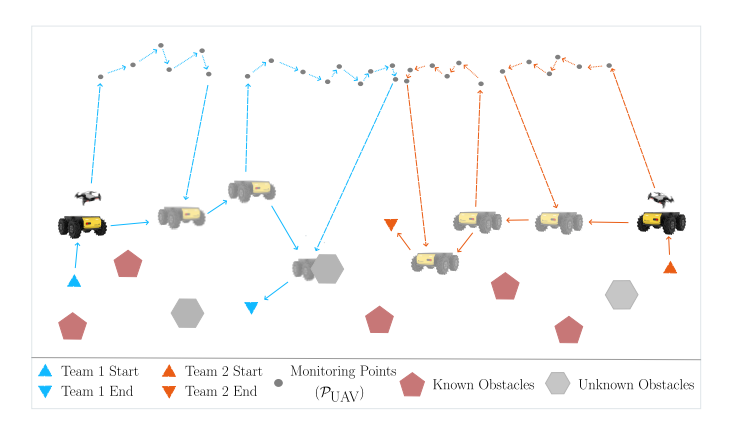


Figure 1: Each team (UAV-UGV pair) has given start/end positions. The goal is to achieve robust offline planning of the UAV-UGV teams to minimize the mission completion time while ensuring all aerial monitoring points are visited by one of the UAVs without violating the UAVs' energy constraints, even under disturbances that cause longer travel times or deviations from the plan.

Let the environment be represented as

$$Q:=\{(x, y, z) \in \mathbb{R}^3 | \ 0 \le x \le \bar{x}, \ 0 \le y \le \bar{y}, \ 0 \le z \le \bar{z}\},\tag{1}$$

which contains a feasible space $Q_f \subseteq Q$ determined by the obstacles that are known a priori. For example, if none of the obstacles are known, then $Q_f = Q$. Furthermore, let Q_f^g and Q_f^a denote the set of feasible points on the ground and in the air, respectively, i.e., $Q_f^g = \{(x,y,z) \in Q_f | z = 0\}$, and $Q_f^a = Q_f \setminus Q_f^g$. We assume that both Q_f and its subset on the ground Q_f^g are connected, meaning that there exists a feasible path between any pair of points within the respective sets. This is just a mild assumption to ensure the feasibility of the monitoring mission, as otherwise part of the environment would be inaccessible to the vehicles. We define $\ell: Q_f \times Q_f \to \mathbb{R}_{\geq 0}$ as a function that returns the distance (length of the shortest path) between any

two points in the feasible space, Q_f . The overall mission goal is for the teams to collectively visit a set of n points in the air, $\mathcal{P}_{\text{UAV}} = \{p_1, \dots, p_n\} \subset Q_f^a$. Let there be m teams (UAV–UGV pairs) indexed by $\mu = \{1, \dots, m\}$, where $m \leq n$. Each team starts from its initial position $p_0^{\mu} \in Q_f^g$ and must reach to its specified final position $p_f^{\mu} \in Q_f^g$. Collectively, the teams must ensure that all points in \mathcal{P}_{UAV} are visited without violating UAVs' energy constraints, while minimizing completion time.

During this mission, the UAVs should never be expected to continuously fly longer than a specified duration due to their energy limitation. To satisfy this requirement, we focus on an approach where the UGVs transport the UAVs through a sequence of points, which we call the *release* and *collect points*. At each release point, the UAV takes-off and visits a subset of \mathcal{P}_{UAV} , then lands on the UGV at the corresponding collect point to be recharged and transported to the next release point (or the respective final position if no more points from \mathcal{P}_{UAV} will be visited by the team). Clearly, a necessary condition for the optimality of such a solution is that the UAV samples at least one point from \mathcal{P}_{UAV} in each tour. Furthermore, each tour can be defined by at most n + 2 points (a release and a collect point, and at most n points from \mathcal{P}_{UAV}). Accordingly, we encode the mission plan of each team $\mu \in \{1, 2, \ldots, m\}$ as a matrix:

$$X^{\mu} = \begin{bmatrix} X_{1,1}^{\mu} & \cdots & X_{1,n+2}^{\mu} \\ \vdots & \ddots & \vdots \\ X_{n,1}^{\mu} & \cdots & X_{n,n+2}^{\mu} \end{bmatrix},$$

where each $X_{i,j}^{\mu} \in Q_f$ denotes a release point if j=1, a collect point if j=n+2, or a point to be visited by the UAV if $j \in \{2,\ldots,n+1\}$. Each row i of X^{μ} (denoted by X_i^{μ}) is used to encode a tour, i.e., the UAV traversing a shortest path along the following sequence of waypoints in that row and meeting with the UGV at $X_{i,n+2}^{\mu}$. Using this, any plan with fewer than n tours can be expressed by having $X_{i,1}^{\mu} = X_{i,2}^{\mu} = \ldots = X_{i,n+2}^{\mu}$ in certain rows of X^{μ} (indicating a "trivial tour" of zero length). After each tour i is completed, the UGV transports the UAV from the collect point $X_{i,n+2}^{\mu}$ to the next release point $X_{i+1,1}^{\mu}$ (or the specified final position p_f^{μ} if i=n) while recharging it. For each team μ , the total time to execute the respective plan X^{μ} is

$$\begin{split} \tau(X^{\mu}) &= \tau_{g}(p_{o}^{\mu}, X_{1,1}^{\mu}) + \tau_{g}(X_{n,n+2}^{\mu}, p_{f}^{\mu}) \\ &+ \sum_{i=1}^{n} \max(\tau_{a}(X_{i}^{\mu}), \tau_{g}(X_{i,1}^{\mu}, X_{i,n+2}^{\mu})) \\ &+ \sum_{i=1}^{n-1} \max(\tau_{g}(X_{i,n+2}^{\mu}, X_{i+1,1}^{\mu}), \tau_{c}(X_{i}^{\mu})), \end{split} \tag{2}$$

where $\tau_a:Q^{n+2}\to\mathbb{R}_{\geq 0}$ and $\tau_g:Q\times Q\to\mathbb{R}_{\geq 0}$ are functions denoting the time to traverse the corresponding paths by the UAV and the UGV, respectively. By definition, τ_a and τ_g equal zero for zero-length paths. Each $\tau_a(X_i^\mu)$ denotes the time required for the μ^{th} UAV to complete the i^{th} tour, starting from its release point $X_{i,1}^\mu$, traversing the following sequence of points in the tour, $X_{i,2}^\mu,\dots,X_{i,n+1}^\mu$, and meeting with the μ^{th} UGV at the collect point $X_{i,n+2}^\mu$. The term $\tau_g(p_o^\mu,X_{1,1}^\mu)$ represents the

time for the μ^{th} UGV to travel from its start position p_0^{μ} to the first release point, whereas $\tau_g(X^{\mu}_{n,n+2},p^{\mu}_{\mathrm{f}})$ denotes the time for the μ^{th} UGV to travel from the final collect point to p_f^{μ} . Similarly, $\tau_g(X_{i,n+2}^{\mu}, X_{i+1,1}^{\mu})$ captures the time spent by the UGV while moving between the collect and release points of consecutive tours i and i + 1, during which the UAV is recharged for the next flight. The third term of the summation in (2) is the total time spent by team μ to complete the specified tours, and the last term is the total time spent between the end and start of consecutive tours of team μ . Here, for each tour i, $\tau_g(X_{i,1}^{\mu}, X_{i,n+2}^{\mu}) \ge 0$ is the time for UGV to go from $X_{i,1}^{\mu}$ to $X_{i,1n+2}^{\mu}$ over a shortest path. Similarly, $\tau_{\rm g}(X_{i,n+2}^{\mu},X_{i+1,1}^{\mu})\geq 0$ is the time for the $\mu^{\rm th}$ UGV to transport the μ^{th} UAV from $X_{i,n+2}^{\mu}$ to $X_{i+1,1}^{\mu}$ over a shortest path. The time to fully recharge¹ the UAV after it completes the tour i is denoted by $\tau_c(X_i^{\mu}) \geq 0$. Since UAVs start the mission fully charged, this ensures that they are fully charged before each tour. We define our robust planning problem as minimizing the maximum mission time among m teams under the mission constraints, i.e.,

$$\min_{\{X^{\mu}\}_{\mu=1}^{m}} \max_{\mu=\{1,\dots,m\}} \tau(X^{\mu}) \tag{3a}$$

s.t.
$$\forall p_k \in \mathcal{P}_{\text{UAV}}, \exists X_{i,j}^{\mu} = p_k,$$
 (3b)

$$\tau_{a}(X_{i}^{\mu}) + \delta_{a} \le \overline{\tau_{a}}, \forall i, \forall \mu,$$
 (3c)

$$\tau_g(X_{i,1}^{\mu}, X_{i,n+2}^{\mu}) + \delta_g \le \overline{\tau_a}, \forall i, \forall \mu, \tag{3d}$$

$$X_{i,1}^{\mu}, X_{i,n+2}^{\mu} \in Q_f^g, \forall i, \forall \mu,$$
 (3e)

$$X_{i,j}^{\mu} \in \mathcal{P}_{\text{UAV}} \cup \{X_{i,j-1}^{\mu}\}, \forall j \in \{2, ..., n+1\}, \forall i, \forall \mu,$$
(3f)

where $\tau(X^{\mu})$ is the total time for team μ to complete its plan as given in (2), and the constraints are as follows: First, (3b) ensures that all points in \mathcal{P}_{UAV} are visited by at least one team. Second, (3c) implies that none of the tours require the respective UAV to fly longer than $\overline{\tau}_a$, even if the time to complete the tour increases by some specified $\delta_a \ge 0$ during the mission due to disturbances. In any tour, if the UAV arrives at the collect location earlier than the UGV, it needs to hover until the UGV's arrival. Accordingly, (3d) ensures that, for any team, the UGV arrives at the collect location before the UAV runs out of energy, even if the ground travel time increases by $\delta_g \geq 0$, playing a similar role for the ground leg as δ_a does for the aerial leg. Here, the choice of robustness parameters, (δ_a, δ_g) , determines how much increase in travel times due to disturbances (e.g., unknown obstacles, terrain, wind) can be tolerated during the mission execution without needing a major revision (changing the tours taken by the UAV) to the resulting plan. Fourth, for any team, (3e) ensures that all the release and collect points are feasible points on the ground. Finally, (3f) ensures that, in any row i of X^{μ} , each entry other than the first and the last ones is either a point from \mathcal{P}_{UAV} or just a repetition of the previous

entry. Accordingly, either all those points are equal to the respective release point $X_{i,1}^{\mu}$ (e.g., a trivial tour) or there exists some $X_{i,j}^{\mu} \neq X_{i,1}^{\mu}$ (i.e., the UAV departs from $X_{i,1}^{\mu}$) such that all the following entries in that row until the collect point are from \mathcal{P}_{UAV} , i.e., $X_{i,j'}^{\mu} \in \mathcal{P}_{\text{UAV}}$ for all $j' \in \{j, \dots, n+1\}$. Note that (3f) does not impose any restriction on how many points from \mathcal{P}_{UAV} can be included in each tour since the respective entries, $X_{i,j'}^{\mu}$ are not necessarily distinct. We denote the overall mission plan as $X = \{X^1, \dots, X^m\}$, representing the collection of all feasible team plans, where team μ 's plan is denoted by X^{μ} .

Definition 1. (Tour Robustness) For any a feasible mission plan $X = \{X^1, ..., X^m\}$, the robustness of the i^{th} tour of the μ^{th} team is given by the maximum increases in the travel times of the UAV/UGV in that tour that do not violate UAVs' energy limitations encoded in (3c),(3d):

$$\hat{\delta}_a^{\mu,i}(X) = \overline{\tau_a} - \tau_a(X_i^{\mu}),$$

$$\hat{\delta}_g^{\mu,i}(X) = \overline{\tau_a} - \tau_g(X_{i,1}^{\mu}, X_{i,n+2}^{\mu}).$$

For any feasible X, since (3c) and (3d) are satisfied for every team μ and every tour i, δ_a and δ_g in (3) impose lower bounds on the robustness of every tour, i.e., $\delta_a^{\mu,i}(X) \ge \delta_a$ and $\delta_g^{\mu,i}(X) \ge \delta_g$ for every i and μ . Accordingly, the robustness parameters δ_a and δ_g in (3) can be tuned to achieve a desired trade-off between robustness and efficiency. Selecting larger values of δ_a and δ_a leads to a plan X with more robust tours, but it also reduces the feasible space of the planning problem, potentially leading to solutions with higher cost mission times. For example, if many/large unknown ground obstacles are anticipated, a larger δ_g can be selected, which effectively forces the release and collect points to be closer together for caution. Analogously, it would be desirable to select δ_a as the maximum possible increase in the UAVs' travel times during tours, accounting for both potential changes in the release/collect points due to obstacles and in-flight disturbances (obstacles, wind, etc.).

3. Proposed Solution

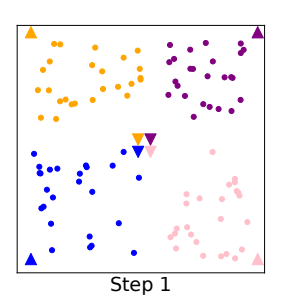
The robust planning problem given in (3) is a mixed-integer program (MIP), which is NP-Hard. Hence, exact solution methods (e.g., Branch & Cut [16]) are computationally intractable with large $|\mathcal{P}_{\text{UAV}}|$. We propose a scalable and efficient heuristic to overcome this challenge. In this section, we present our approach and its formal performance guarantees.

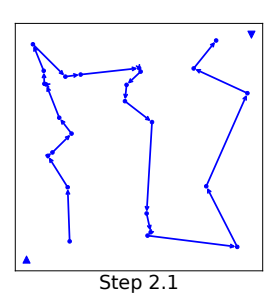
3.1. Proposed Robust Planning Algorithm

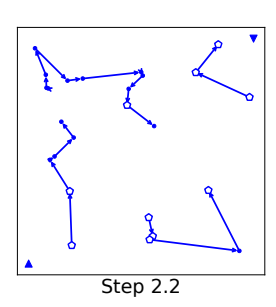
Our proposed algorithm, Alg.1, uses the fact that (3) share structural similarity with multiple Traveling Salesperson Problem (mTSP). The mTSP is a generalization of TSP, where multiple agents collectively visit all nodes while minimizing overall cost. In our setting, there are additional constraints that stem from the limitations of UAV-UGV teams. Our approach consists of 2 steps, as illustrated in the example shown in Fig. 2.

 $^{^1}$ As an alternative to recharging, a battery-swapping approach can also be modeled like this by setting $au_c(X_+^\mu)$ equal to a small constant.









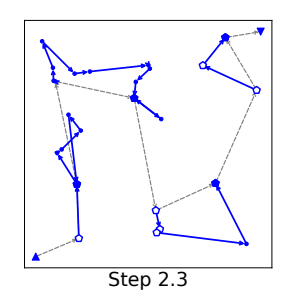


Figure 2: Output of Alg.1 for m=4 teams (Top View). Left: \mathcal{P}_{UAV} (gray points). In Step 1, assigned points to teams are color-coded with upward/downward triangles showing p_p^μ/p_f^μ . Steps 2.1–2.3 show the detailed planning for one of the teams (blue, $\mu=1$). In Step 2.1, the path shows the initial tour over $\mathcal{P}_{\text{UAV}}^\mu$ (blue points from Step 1). Upward and downward blue triangles are the initial and final positions, respectively. In Step 2.2, blue lines are feasible tours for the UAV-UGV team, and hollow pentagons are feasible collect points for each tour. In Step 2.3, the plan is obtained, filled pentagons represent the selected collect point for that tour, and dashed grey lines are the UGV path.

In Step 1, we partition the \mathcal{P}_{UAV} among the m teams. For each UAV point $p_i \in \mathcal{P}_{\text{UAV}}$, the algorithm determines the team that minimizes its distance to either the team's start position p_o^μ or its end position p_f^μ (line 4). The point p_i is then assigned to the corresponding team (line 5). After all points are assigned, the algorithm outputs $\{\mathcal{P}_{\text{UAV}}^\mu\}_{\mu=1}^m$, which together form a partition of \mathcal{P}_{UAV} i.e., $\mathcal{P}_{\text{UAV}} = \bigcup_{\mu=1}^m \mathcal{P}_{\text{UAV}}^\mu$ and $\mathcal{P}_{\text{UAV}}^\mu \cap \mathcal{P}_{\text{UAV}}^\nu = \emptyset$ for $\mu \neq \nu$. In Step 2, we construct a feasible plan for each team μ based

In Step 2, we construct a feasible plan for each team μ based on its assigned $\mathcal{P}_{\text{UAV}}^{\mu}$ from Step 1. The algorithm iterates over all teams $\mu \in \{1, \ldots, m\}$ and, for each team, constructs X^{μ} . This process has 3 sub-steps:

In Step 2.1, we obtain an efficient sequence to visit the points in $\mathcal{P}_{\text{UAV}}^{\mu}$ by treating the problem as a standard TSP, i.e., by ignoring the energy constraint of the UAV and finding the shortest trajectory that visits all the points in $\mathcal{P}_{\text{UAV}}^{\mu}$, starting with the one closest to the initial position p_0^{μ} and ending with the one closest to the final position p_1^{μ} . This step can be achieved using any state-of-art heuristic; we use the Christofides Algorithm [17].

In Step 2.2, we obtain a feasible plan X^{μ} for team μ , (the collection of all such plans, $X = \{X^1, \dots, X^m\}$, constitutes a feasible solution to (3)) by breaking the output of Step 2.1, S^{μ} , into maximal tours that are feasible both for the μ^{th} energy-limited UAV and the μ^{th} UGV. Starting with i = 1, we iteratively build each row i of X^{μ} . If all the points in S^{μ} have already been added to X^{μ} , no further tours are needed, and we set $X_{i,1}^{\mu}$ to $X_{i-1,1}^{\mu}$ (lines 15-16). Otherwise, $X_{i,1}^{\mu}$ is set to $\pi(S_k^{\mu}) = \arg\min_{p \in Q_{\varepsilon}^g} \ell(p, S_k^{\mu})$, the closest feasible point on the ground to S_{ν}^{μ} , i.e. the next point in S^{μ} (line 17-18). We set the collect point of current tour as the release point, serving as a valid default structure (line 19). For the remaining entries in the row, i.e., each $X_{i,j}^{\mu}$ for $n_{\mu}+1 \ge j \ge 2$, if all the points in S^{μ} have already been visited $(k = n_{\mu} + 1)$, then $X_{i,j} = X_{i,j-1}$, which implies no motion (line 33). Otherwise (lines 22-31), we add S_k^{μ} to the current tour, and create a set of feasible collect points, C. Specifically, for each candidate collect point $\pi(X_{i,r}^{\mu})$ $(2 \le r \le j)$, we check:

- 1. Whether the UAV can complete its tour and land at $\pi(X_{i,r}^{\mu})$ before violating its battery constraint, (3c).
- 2. Whether the UGV can meet the UAV at $\pi(X_{i,r}^{\mu})$ before the UAV's battery is depleted (3d).

Note that $\pi(X_{i,2}^{\mu}) = X_{i,1}^{\mu}$. Therefore, we are checking all the

points in current tour as possible collect points. If both conditions are satisfied, we add $\pi(X_{i,r}^{\mu})$ to C. If C is non-empty, there is at least one feasible collect point. In that case, we store C as C_i^{μ} , the set of feasible collect points for the i^{th} tour. Otherwise, we remove S_k^{μ} from the tour and copy the previous point.

In Step 2.3, we select the best collect point for each tour by solving a Generalized Traveling Salesman Problem (GTSP). The objective is to minimize team μ 's plan execution time, $\tau(X^{\mu})$. GTSP extends TSP by enforcing the agent to visit exactly one node from each cluster. Here, the clusters are the feasible collect points $C_1^{\mu}, \ldots, C_{n_{\mu}}^{\mu}$ obtained in Step 2.2. All other nodes (the release points, p_o^{μ} and p_f^{μ}) are treated as clusters with a single node and therefore always chosen. We create the graph as follows (lines 35-45):

- Add nodes for p_o^{μ} , p_f^{μ} , all release points and all feasible collect points for each tour.
- Connect p_o^{μ} to the first release point $X_{1,1}^{\mu}$ with an edge weighted by the UGV travel time between them.
- Connect the release point of each tour to each of its feasible collect points, with the edge weight being the maximum of the UAV's tour time and UGV travel time from the release to the collect point.
- Connect each feasible collect point to the release point of the next tour (or p_f^{μ} in the case of the last tour), with an edge weight equal to the maximum of the UGV's travel time and the UAV's recharge time after previous tour.

With this structure, the resulting GTSP solution has the form $(p_o^\mu, X_{1,1}^\mu, c_1^\mu, \dots, X_{n,1}^\mu, c_{n_\mu}^\mu, p_f^\mu)$, where c_i^μ is the selected collect point for i^{th} tour from C_i^μ . In line 46, we solve the GTSP using the GLNS heuristic [18] with a bounded runtime of σn_μ^3 where σ is a user-defined constant, and $n_\mu = |\mathcal{P}_{\text{UAV}}^\mu|$. Note that we have fixed the start and end node. This procedure returns the optimized collect points $(c_1^\mu, \dots, c_{n_\mu}^\mu)$. Finally, we complete X^μ by setting $X_{i,n_\mu+2}^\mu$ to c_i^μ for all $1 \le i \le n_\mu$ (line 48). After X^μ is completed, it is added to the overall mission plan X (line 49).

Theorem 1. Alg.1 returns a feasible solution to (3) if one exists, and it has the worst-case time complexity of $O(mn + n^3)$,

```
Algorithm 1: RSPECT, Robust Multi UAV-UGV Planning Algorithm
      Input: \mathcal{P}_{UAV} (Set of n points to visit), m (Number of teams),
                        \{p_o^\mu\}_{\mu=1}^m, \{p_f^\mu\}_{\mu=1}^m (Team Start/Finish positions), \ell (Distance
                        function) Q_f^g (Feasible Ground Space), Q_f^a (Feasible Air
                        Space), \tau_a, \tau_g (UAV, UGV travel time functions), \tau_g (UGV
                        travel time function), \overline{\tau_a} (Maximum flight time), \delta_a, \delta_g
                        (Robustness parameters), \sigma (GLNS time limit constant)
      Output: X = \{X^{\mu}\}_{\mu=1}^{m} (Mission Plan)
 1 Step 1: Assign points to the teams
 2 Initialize: \{\mathcal{P}_{\text{UAV}}^{\mu}\}_{\mu=1}^{m} \leftarrow \varnothing
 3 for i \leftarrow 1 to n do
              \begin{split} \boldsymbol{\mu^{\star}} &\leftarrow \arg\min_{\boldsymbol{\mu} \in \{1, \dots, m\}} \min \left( \ell(p_i, p_o^{\boldsymbol{\mu}}), \ell(p_i, p_f^{\boldsymbol{\mu}}) \right) \\ \boldsymbol{\mathcal{P}_{\mathrm{UAV}}^{\boldsymbol{\mu^{\star}}}} &\leftarrow \boldsymbol{\mathcal{P}_{\mathrm{UAV}}^{\boldsymbol{\mu^{\star}}}} \cup \{p_i\} \end{split}
     Step 2: Generate feasible plans for each team
     Initialize: X \leftarrow \emptyset
7
      for \mu \leftarrow 1 to m do
               n_{\mu} \leftarrow |\mathcal{P}_{\text{UAV}}^{\mu}|
 9
10
               Step 2.1: Find an approximate solution S^{\mu} to TSP on \mathcal{P}_{\text{UAV}}^{\mu}
                Use an approximate TSP solver [17]^2 on \mathcal{P}_{UAV}^{\mu} to find \mathcal{S}^{\mu} such
11
                  that S_1^{\mu} = arg min \ell(p_0^{\mu}, p), S_{n_{\mu}} = arg min \ell(p_f^{\mu}, p)
                                                                                p \in \mathcal{P}_{UAV}^{\mu}
               Step 2.2: Create feasible tours from the sequence S^{\mu}
12
                Initialize: X^{\mu} \leftarrow \emptyset, k \leftarrow 1
13
               for i \leftarrow 1 to n_{\mu} do
14
                        if k = n_{\mu} + 1 then
X_{i,1}^{\mu} \leftarrow X_{i-1,1}^{\mu}
15
16
                        else
X_{i,1}^{\mu} \leftarrow \pi(S_k^{\mu}) = \underset{p \in Q_f^g}{\arg\min} \ell(p, S_k^{\mu})
17
18
                         X_{i,n_{\mu}+2}^{\mu} \leftarrow X_{i,1}^{\mu}
19
                         for j \leftarrow 2 to n_{\mu} + 1 do
20
                                 if k \leq n_{\mu} then
X_{i,j}^{\mu} \leftarrow \mathcal{S}_{k}^{\mu}
22
23
                                            for r \leftarrow 2 to j do
24
                                                     if \tau_a(X_i^{\mu}) + \delta_a \leq \overline{\tau_a} and \tau_g(X_{i,1}^{\mu}, \pi(X_{i,r}^{\mu})) + \delta_g \leq \overline{\tau_a}
25
                                                         C \leftarrow C \cup \{\pi(X_{i,r}^{\mu})\} 
 26
                                            if C \neq \emptyset then
27
                                                  C_i^{\mu} \leftarrow Ck \leftarrow k + 1
28
29
                                          else X_{i,j}^{\mu} \leftarrow X_{i,j-1}^{\mu}
30
31
32
                                     X_{i,j}^{\mu} \leftarrow X_{i,j-1}^{\mu}
33
               Step 2.3: Create a feasible plan X^{\mu} using GTSP
34
                V^{\mu} \leftarrow \bigcup_{i} (C_{i}^{\mu} \cup \{X_{i,1}^{\mu}\}) \cup \{p_{o}^{\mu}, p_{f}^{\mu}\}
35
               G^{\mu} \leftarrow \operatorname{Graph}(V^{\mu})
36
               G^{\mu}.add_edge(p_o^{\mu}, X_{i,1}^{\mu}, \tau_g(p_o^{\mu}, X_{1,1}^{\mu}))
37
38
               for i \leftarrow 1 to n_{\mu} do
                         foreach c \in C_i^{\mu} do
39
                                  X_{i,n_{\mu}+2}^{\mu} \leftarrow^{\iota} c
40
                                  G^{\mu}.add_edge(X_{i,1}^{\mu}, c, \max[\tau_g(X_{i,1}^{\mu}, c), \tau_a(X_i^{\mu})])
41
42
                                           G^{\mu}.add_edge(c, p_f^{\mu}, \max[\tau_g(c, p_f^{\mu}), \tau_c(X_i^{\mu})])
43
44
                                  else
                \begin{vmatrix} & & G^{\mu}.\text{add\_edge}(c, X_{i+1,1}^{\mu}, \max[\tau_{g}(c, X_{i+1,1}^{\mu}), \tau_{c}(X_{i}^{\mu})]) \\ (c_{1}^{\mu}, \dots, c_{n_{\mu}}^{\mu}) \leftarrow \text{GLNS}(G^{\mu}, p_{o}^{\mu}, p_{f}^{\mu}, \{C_{1}^{\mu}, \dots, C_{n_{\mu}}^{\mu}\}, \sigma) [18]^{2} \end{vmatrix} 
45
46
               for i \leftarrow 1 to n_{\mu} do
47
                        X_{i,n_{\mu}+2}^{\mu} = c_i^{\mu}
               X \leftarrow X \cup \{X^{\mu}\}
49
     return X
```

where m is the number of UAV-UGV teams and $n = |\mathcal{P}_{UAV}|$ is the number of monitoring points.³

Proof. (Feasibility:) In Step 1, Alg.1 partitions \mathcal{P}_{UAV} among mteams, guaranteeing each monitoring point is assigned to exactly one team i.e., $\mathcal{P}_{\text{UAV}} = \bigcup_{\mu=1}^{m} \mathcal{P}_{\text{UAV}}^{\mu}$ and $\mathcal{P}_{\text{UAV}}^{\mu} \cap \mathcal{P}_{\text{UAV}}^{\nu} = \emptyset$ for $\mu \neq \nu$. In line 11, Alg.1 solves a TSP on $\mathcal{P}_{\text{UAV}}^{\mu}$, which guarantees that all the points in $\mathcal{P}_{\text{UAV}}^{\mu}$ are included in the generated sequence \mathcal{S}^{μ} . In the lines 15-19, $X_{i,1}^{\mu}$ is either chosen as a point in Q_f^g or as the release point of the previous tour. In either case, $X_{i,1}^{\mu}$ satisfies (3e). In Step 2, lines 20-33, each S_k^{μ} is added to the current tour (row i) if the there is a collect point for which the resulting tour would not violate (3c) and (3d). Note that if a feasible solution to (3) exists, then each $p \in \mathcal{P}_{UAV}$ must be reachable from the closest feasible point on the ground without violating the constraint (3c). Hence, under Alg.1, for each run of the main for loop in Step 2, unless $k > n_{\mu}$, at least one waypoint S_k^{μ} is added to the plan matrix of the team, X^{μ} (as in line 22). Since X^{μ} has $n_{\mu} = |S^{\mu}|$ rows, this means that all the waypoints in S^{μ} will be included in X^{μ} created by Alg.1. Moreover, if there are no remaining points in S^{μ} , i.e., $k > n_{\mu}$, or adding S_k to tour i would violate (3c) or (3d), then $X_{i,i}^{\mu}$ is assigned to be the same as the previous point $X_{i,j-1}^{\mu}$ (for $j \le n_{\mu} + 1$, lines 31 and 33). Hence, (3f) is also satisfied. In Step 3, collect points for each tour are chosen from a set of points which all satisfy (3d) and (3e). Finally, the mission plan $X = \{X^{\mu}\}_{\mu=1}^{m}$ satisfies (3b) collectively since $\mathcal{P}_{\text{UAV}} = \bigcup_{\mu=1}^{m} \mathcal{P}_{\text{UAV}}^{\mu}$ and thus constitutes a feasible solution to (3).

(Complexity:) In Step 1, the for loop runs n times. In this loop, all operations take linear time with respect to m. Thus, the runtime of Step 1 is O(mn).

Steps 2.1–2.3 are executed once per team. In each run μ of Step 2.1 of Alg.1, we utilize the Christofides algorithm, which has a time complexity of $O(n_{\mu}^{3})$, where $n_{\mu} = |\mathcal{P}_{\text{UAV}}^{\mu}|$. Enforcing the start and end points $(\mathcal{S}_{1}^{\mu} \text{ and } \mathcal{S}_{n_{\mu}}^{\mu})$ as in line 11 of Alg.1 does not affect the time-complexity of the Christofides algorithm. Time complexity of projection function $\pi(.)$ in line 18 depends on the definition of obstacles that are known a priori. Clearly, the obstacles that are unknown a priori has no impact on this offline computation. Assuming that the known obstacles are expressed as convex polytopes, finding the closest point on the boundary of such polytope to an interior point can be formulated as a convex quadratic program for each face, which is solvable in polynomial time in the number of faces and the dimension of the space [19]. Checking if a point is inside a convex polytope reduces to a linear programming feasibility problem and is therefore polynomial-time solvable. Therefore, if there are b such obstacles, the total cost of a projection scales as O(b), assuming each obstacle has a bounded number of faces. So the total time to find the ground projections of all n_{μ} monitoring points assigned to team μ is $O(n_{\mu}b)$, which is dominated

²Other TSP/GTSP solvers can be used in these steps. However, this might change the worst-case time complexity of Alg.1 given in Theorem 1.

³In practice, the number of monitoring points (n) is typically much larger than the number of UAV-UGV teams (m). Hence, the worst-case complexity of Alg.1, $O(mn + n^3)$, is usually dominated by the growth of n as $O(n^3)$.

by the runtime of Step 2.1, $O(n_{\mu}^{3})$, assuming that the number of known obstacles *b* is bounded.

In Step 2.2 of Alg.1, all for loops iterate at most n_{μ} times. While this step includes projection operations, their costs have already been accounted for in the overall projection time discussed earlier. All remaining operations within these loops take constant time. Consequently, the time complexity of Step 2.2, excluding projections, is $O(n_{\mu}^{3})$.

In Step 2.3 of Alg.1, we use GLNS to solve the GTSP. Although GLNS does not have worst-case polynomial-time complexity, we have restricted its runtime to $O(n_{\mu}^{3})$ by enforcing a time limit of σn_{μ}^{3} , where σ is a user-defined constant.

Steps 2.1–2.3 are executed once per team. Since the overall runtime of these steps for each team μ is $O(n_{\mu}^{3})$, the total runtime of Step 2 will be $\sum_{\mu=1}^{m} O(n_{\mu}^{3})$. Since $\{\mathcal{P}_{\text{UAV}}^{\mu}\}_{\mu=1}^{m}$ is a prtition of \mathcal{P}_{UAV} , we have $\sum_{\mu=1}^{m} n_{\mu} = n$ and $n_{\mu} \geq 0$. For any set of non-negative numbers, the sum of their cubes is less than or equal to cube of their sum. This gives the inequality $\sum_{\mu=1}^{m} n_{\mu}^{3} \leq (\sum_{\mu=1}^{m} n_{\mu})^{3}$, which simplifies to $\sum_{\mu=1}^{m} n_{\mu}^{3} \leq n^{3}$. Hence the worst-case complexity of Step 2 is $O(n^{3})$. Combining this with the complexity of Step 1, O(mn), we obtain the the overall complexity of Alg.1 as $O(mn+n^{3})$.

3.2. Robustness Analysis

Among the various sources of uncertainty, a priori unknown obstacles are arguably one of the most common and significant ones. Such unknown obstacles may render certain release/collect points in $X=\{X^\mu\}_{\mu=1}^m$ inaccessible to UGVs during actual execution and/or increase traverse time by the UAVs/UGVs during each tour. However, if X has sufficient tour robustness values, i.e., $\hat{\delta}_a^{\mu,i}(X)$ and $\hat{\delta}_g^{\mu,i}(X)$ are sufficiently large, it may still be possible to follow the plan by only making small modifications in the release/collect points (as opposed to a complete replaning). In this section, we formally analyze the robustness of our method to such unknown obstacles.

Let $\tilde{Q}_f \subseteq Q_f$ be the actual feasible space, i.e., the feasible points remaining after the a priori unknown obstacles are removed from Q_f . Accordingly, let $\tilde{Q}_f^g \subseteq Q_f^g$ be the set of actual feasible points on ground. Same as before, we assume that both \tilde{Q}_f and \tilde{Q}_f^g are connected sets. Moreover, $\mathcal{P}_{\text{UAV}} \subseteq \tilde{Q}_f$. These mild assumptions imply that the mission is still achievable within the actual feasible space. Furthermore, let $\tilde{\tau}_a: \tilde{Q}_f^{n+2} \to \mathbb{R}_{\geq 0}$ and $\tilde{\tau}_g: \tilde{Q}_f \times \tilde{Q}_f \to \mathbb{R}_{\geq 0}$ be actual traversal-time functions i.e., the times required for the UAVs and UGVs to traverse the corresponding paths within the actual feasible space \tilde{Q}_f . Finally, let $\tilde{X} = \{\tilde{X}^\mu\}_{\mu=1}^m$ be any modified overall plan. In the following theorem, we state sufficient conditions under which the plan generated by Alg. 1, $X = \{X^\mu\}_{\mu=1}^m$, can be executed in the face of unknown obstacles by simply adjusting the release and collect points as needed.

Theorem 2. Let $X = \{X^{\mu}\}_{\mu=1}^{m}$ be a feasible solution to (3) with tour robustness values $\hat{\delta}_{a}^{\mu,i}(X), \hat{\delta}_{g}^{\mu,i}(X)$ (see Def.1), and let $\tilde{X} = \{\tilde{X}^{\mu}\}_{u=1}^{m}$ be a modified overall plan such that

• Each \tilde{X}^{μ} differs from X^{μ} only in its release and collect points, i.e., $\tilde{X}^{\mu}_{i,1}, \tilde{X}^{\mu}_{i,n_{\mu}+2} \in \tilde{Q}^{g}_{f}$ and $X^{\mu}_{i,1}, X^{\mu}_{i,n_{\mu}+2} \in Q^{g}_{f}$.

• The following holds for each \tilde{X}^{μ} and $\forall i = \{1, ..., n_{\mu}\}$:

$$\tilde{\tau}_a(\tilde{X}_i^{\mu}) \le \tau_a(X_i^{\mu}) + \hat{\delta}_a^{\mu,i}(X),\tag{4}$$

$$\tilde{\tau}_{g}(\tilde{X}_{i,1}^{\mu}, \tilde{X}_{i,n_{u}+2}^{\mu}) \le \tau_{g}(X_{i,1}^{\mu}, X_{i,n_{u}+2}^{\mu}) + \hat{\delta}_{g}^{\mu,i}(X), \tag{5}$$

where $n_{\mu} = |\mathcal{P}_{UAV}^{\mu}|$. Then under \tilde{X} , every point in \mathcal{P}_{UAV} is visited while respecting the energy limitation of the UAVs, i.e., $\tilde{\tau}_a(\tilde{X}_i^{\mu}) \leq \overline{\tau_a}$ and $\tilde{\tau}_g(\tilde{X}_{i,1}^{\mu}, \tilde{X}_{i,n_{\mu}+2}^{\mu}) \leq \overline{\tau_a}$ for all $i = \{1, ..., n_{\mu}\}$ and $\mu = \{1, ..., m\}$.

Proof. As a feasible solution to (3), X satisfies (3b), and UAVs visit all points in \mathcal{P}_{UAV} under X. Since X and \tilde{X} only differ in release and collect points, the UAVs visit all points in \mathcal{P}_{UAV} also under \tilde{X} . By Def. 1, for all i and μ , we have:

$$\tau_a(X_i^{\mu}) + \hat{\delta}_a^{\mu,i}(X) \le \overline{\tau_a},\tag{6}$$

$$\tau_g(X_{i,1}^{\mu}, X_{i,n_{\mu}+2}^{\mu}) + \hat{\delta}_g^{\mu,i}(X) \le \overline{\tau_a}.$$
 (7)

Using (4) and (6) gives $\tilde{\tau}_a(\tilde{X}_i^{\mu}) \leq \overline{\tau_a}$. Similarly, using (5) and (7) gives $\tilde{\tau}_g(\tilde{X}_{i,1}^{\mu}, \tilde{X}_{i,n_{\mu}+2}^{\mu}) \leq \overline{\tau_a}$. Consequently, under \tilde{X} , all points in \mathcal{P}_{UAV} are visited while respecting the energy limits of the UAVs.

3.3. Special Case: VTOL UAV, Unknown Ground Obstacles

In light of Theorem 2, when obstacles on the ground are the primary source of uncertainty, an offline overall plan $X = \{X^{\mu}\}_{\mu=1}^{m}$ with sufficiently robust tours allows the UAV-UGV teams to complete the mission by only adjusting their own release/collect points if needed, without any other changes to $X = \{X^{\mu}\}_{\mu=1}^{m}$. Under some mild conditions on the vehicles and the environment, as given in Assumption 1, this online modification of the release/collect points becomes even simpler: feasible points within a certain radius, which depends on $\hat{\delta}_a^{\mu,i}(X)$, from the original release/collect points can be used as the modified release/collect points as long as the resulting travel time of UGV between those release and collect points are not increased by more than $\hat{\delta}_g^{\mu,i}(X)$ relative to X.

Assumption 1. ⁴ UAVs can perform vertical take-off/landing (VTOL) at any feasible ground point to/from a minimum flight altitude \underline{z} in constant time τ_{TL} . No obstacles prevent VTOL or exist at altitudes higher than z.

Corollary 1. Let Assumption 1 hold, let $X = \{X^{\mu}\}_{\mu=1}^{m}$ be a feasible solution to (3) with robustness $\hat{\delta}_{a}^{\mu,i}(X), \hat{\delta}_{g}^{\mu,i}(X)$, and let $\tilde{X} = \{\tilde{X}^{\mu}\}_{\mu=1}^{m}$ be any modified plan that differs from X only in

⁴Note that Assumption 1 is not required for our generic results in Theorems 1 and 2. It is only utilized in Corollary 1, which enables a simple, local plan modification strategy for the UAV-UGV teams in response to ground obstacles (Remark 1). The VTOL capability is typical for multi-rotor UAVs, whose take-off and landing maneuvers are usually repeatable within a constant duration τ_{TL} . Obstacle-free VTOL can be achieved when the obstacles are represented via their bounding boxes. The increase in flight time due to obstacles above the minimum flight altitude z is typically negligible when z is sufficiently large.

some release/collect points while satisfying the following conditions for all $\mu = \{1, ..., m\}$ and $i = \{1, ..., n_{\mu}\}$:

$$\|\tilde{X}_{i,1}^{\mu} - X_{i,1}^{\mu}\| + \|\tilde{X}_{i,n_{u}+2}^{\mu} - X_{i,n_{u}+2}^{\mu}\| \le v_{H}^{avg} \cdot \hat{\delta}_{a}^{\mu,i}(X), \tag{8}$$

$$\tilde{\ell}_{g,i}^{\mu} \le \ell_{g,i}^{\mu} + \nu_g^{avg} \cdot \hat{\delta}_g^{\mu,i}(X),\tag{9}$$

where v_H^{avg} is the average speed the UAV can sustain along any fixed-altitude path, v_g^{avg} is the average speed that can be sustained by the UGV, $\ell_{g,i}^{\mu}$ and $\tilde{\ell}_{g,i}^{\mu}$ denote the lengths of shortest feasible ground paths between release and collect points of μ^{th} team's i^{th} tour under X and \tilde{X} . Then under \tilde{X} , every point in \mathcal{P}_{UAV} is visited while respecting the energy limitation of the UAVs, i.e., $\tilde{\tau}_a(\tilde{X}_i^{\mu}) \leq \overline{\tau_a}$ and $\tilde{\tau}_g(\tilde{X}_{i-1}^{\mu}, \tilde{X}_{i-1-2}^{\mu}) \leq \overline{\tau_a}$ for all μ and i.

Proof. We will show that, under Assumption 1, (8) and (9) imply (4) and (5) given in the premise of Theorem 2.

For any X and \tilde{X} satisfying the premise, let's consider each non-trivial tour (rows with at least one point in \mathcal{P}_{UAV}) under the VTOL behavior in Assumption 1. Without loss of generality, let's assume that these non-trivial tours i contain no repetitions of the release point, i.e., $X_{i,j}^{\mu} = \tilde{X}_{i,j}^{\mu} \in \mathcal{P}_{UAV}$ for all $j \in \{2, \ldots, n_{\mu} + 1\}$. Furthermore, since no obstacles prevent vertical take-off/landing or exist above the minimum flight altitude under Assumption 1, we can express the times for such non-trivial tours as:

$$\begin{split} &\tau_{a}(X_{i}^{\mu}) = 2\tau_{TL} + \Delta(X_{i,1}^{\mu}, X_{i,2}^{\mu}) + \Delta(X_{i,2}^{\mu}, X_{i,3}^{\mu}) + \dots + \Delta(X_{i,n_{\mu}+1}^{\mu}, X_{i,n_{\mu}+2}^{\mu}), \\ &\tilde{\tau}_{a}(\tilde{X}_{i}^{\mu}) = 2\tau_{TL} + \Delta(\tilde{X}_{i,1}^{\mu}, X_{i,2}^{\mu}) + \Delta(X_{i,2}^{\mu}, X_{i,3}^{\mu}) + \dots + \Delta(X_{i,n_{\mu}+1}^{\mu}, \tilde{X}_{i,n_{\mu}+2}^{\mu}), \end{split}$$

where the function Δ gives the minimum time it takes a UAV to travel between the respective points, and $X^{\mu}_{i,1}$, $\tilde{X}^{\mu}_{i,1}$ and $X^{\mu}_{i,n_{\mu}+2}$, $\tilde{X}^{\mu}_{i,n_{\mu}+2}$ are the additional waypoints due to VTOL. For example, $X^{\mu}_{i,1}$ is at the minimum flight altitude \underline{z} with the same x and y coordinates as the release point $X^{\mu}_{i,1}$. In both equations above, total time for take-off and landing takes constant time $2\tau_{TL}$. Additionally, in both cases, the time to traverse $X^{\mu}_{i,2},\ldots,X^{\mu}_{i,n_{\mu}+1}$ are equal (no obstacles above \underline{z}). Accordingly,

$$\tilde{\tau}_{a}(\tilde{X}_{i}^{\mu}) - \tau_{a}(X_{i}^{\mu}) = \Delta(\tilde{X}_{i,1}^{\mu}, X_{i,2}^{\mu}) + \Delta(X_{i,n_{\mu}+1}^{\mu}, \tilde{X}_{i,n_{\mu}+2}^{\mu}) - \Delta(X_{i,1}^{\mu}, X_{i,2}^{\mu}) - \Delta(X_{i,n_{\mu}+1}^{\mu}, X_{i,n_{\mu}+2}^{\mu}).$$

$$(10)$$

Moreover, since Δ denotes the minimum travel time between two points, it satisfies the triangle inequality, i.e., for any three points $p_1, p_2, p_3, \Delta(p_1, p_2) \le \Delta(p_1, p_3) + \Delta(p_3, p_2)$. Hence,

$$\Delta(\tilde{X}_{i,1}^{\mu}, X_{i,2}^{\mu}) \le \Delta(\tilde{X}_{i,1}^{\mu}, X_{i,1}^{\mu}) + \Delta(X_{i,1}^{\mu}, X_{i,2}^{\mu}),$$
(11)

$$\Delta(X_{i,n_{\mu}+1}^{\mu},\tilde{X}_{i,n_{\mu}+2}^{\mu}) \leq \Delta(\tilde{X}_{i,n_{\mu}+2}^{\mu},X_{i,n_{\mu}+2}^{\mu}) + \Delta(X_{i,n_{\mu}+1}^{\mu},X_{i,n_{\mu}+2}^{\mu}). \tag{12}$$

Using (10), (11), and (12), we obtain:

$$\tilde{\tau}_{a}(\tilde{X}_{i}^{\mu}) - \tau_{a}(X_{i}^{\mu}) \leq \Delta(\tilde{X}_{i,1}^{\mu}, X_{i,1}^{\mu}) + \Delta(\tilde{X}_{i,n_{\mu}+2}^{\mu}, X_{i,n_{\mu}+2}^{\mu}). \tag{13}$$

Since the distance between the respective release/collect points under X and \tilde{X} are equal to the distance between the projections of those points at the minimum flight altitude, i.e., $\|\tilde{X}_{i,1} - X_{i,1}\| = \|\tilde{X}_{i,1} - X_{i,1}\|$ and

 $\|\tilde{X}_{i,n+2} - X_{i,n+2}\| = \|\tilde{X}_{i,n+2} - X_{i,n+2}\|,$ (13) implies

$$\tilde{\tau}_{a}(\tilde{X}_{i}) - \tau_{a}(X_{i}) \le \frac{\|\tilde{X}_{i,1}^{\mu} - X_{i,1}^{\mu}\|}{v_{H}^{\text{avg}}} + \frac{\|\tilde{X}_{i,n_{\mu}+2}^{\mu} - X_{i,n_{\mu}+2}^{\mu}\|}{v_{H}^{\text{avg}}},$$
(14)

where v_H^{avg} is the the average speed the UAV can sustain along any fixed-altitude path. Using (8) and (14), we obtain

$$\tilde{\tau}_a(\tilde{X}_i^{\mu}) - \tau_a(X_i^{\mu}) \le \hat{\delta}_a^{\mu,i}(X). \tag{15}$$

Hence, \tilde{X} satisfies (4) of Theorem 2. Furthermore, for the UGVs, using v_g^{avg} , we can write:

$$\tilde{\tau}_{g}(\tilde{X}_{i,1}^{\mu}, \tilde{X}_{i,n_{\mu+2}}^{\mu}) - \tau_{g}(X_{i,1}^{\mu}, X_{i,n_{\mu+2}}^{\mu}) \le \frac{\tilde{\ell}_{g,i}^{\mu} - \ell_{g,i}^{\mu}}{v_{g}^{\text{avg}}}.$$
 (16)

Using (9) and (16) together, we have

$$\tilde{\tau}_g(\tilde{X}_{i,1}^{\mu}, \tilde{X}_{i,n_{u+2}}^{\mu}) - \tau_g(X_{i,1}^{\mu}, X_{i,n_{u+2}}^{\mu}) \le \hat{\delta}_g^{\mu,i}(X). \tag{17}$$

Accordingly, \tilde{X} also satisfies (5) of Theorem 2. Hence, using Theorem 2, we can conclude that every point in \mathcal{P}_{UAV} is visited under \tilde{X} while respecting the energy limitations of the UAVs.

Remark 1. Corollary 1 shows that, under Assumption 1, UAV-UGV teams can follow the offline plan X by only changing the release/collect points if they are occupied as long as

- The combined deviation of modified release and collect points from the offline plan remain within $v_H^{avg} \cdot \hat{\delta}_a^{\mu,i}(X)$.
- The ground path length between the modified release and collect points increases by no more than $v_q^{avg} \cdot \hat{\delta}_q^{\mu,i}(X)$.

Figure 3 provides a visualization of these two conditions.

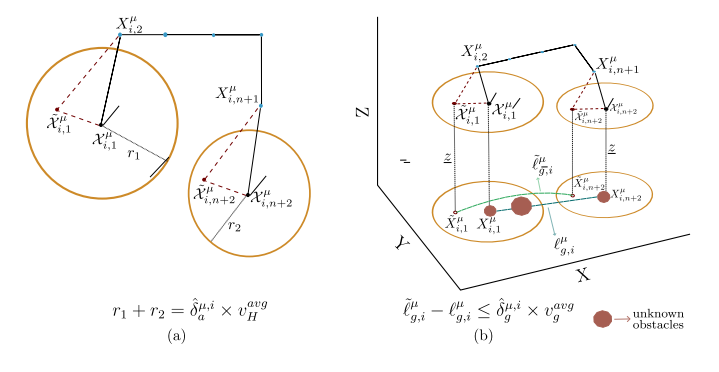


Figure 3: Illustration for Remark 1. A tour with its original and modified release/collect points due to unknown obstacles. (a) top view, (b) 3D view.

4. Simulations

We evaluate the performance and scalability of our proposed method (Alg.1) by comparing it to six different algorithms: 1)

Branch and Cut [16], 2) two metaheuristics—Simulated Annealing (SA) and Genetic Algorithm (GA), and 3) three heuristic methods from the literature ([10, 12, 11]) that were developed for energy-aware planning of UAV-UGV teams. All implementations were performed using Python, Intel i9-13900H CPU, and 16GB RAM. In all these simulations, we consider a VTOL UAV with a minimum flight altitude of \underline{z} =100 m (see Assumption 1). In practice, most UAVs move horizontally at speeds greater than their vertical speeds [20], which is consistent with our configuration (Table 1).

For different values of m (number of UAV-UGV teams) and n (number of monitoring points), 25 random \mathcal{P}_{UAV} were created with a fixed z-coordinate equal to \underline{z} inside a cuboid environment, as defined in (1), with $\bar{x} = \bar{y} = 4000 \, m$. Unless otherwise specified, for each value of m and n, the computation time and the overall mission time $\max_{\mu} \tau(X^{\mu})$ were reported with mean \pm standard deviation over those 25 realizations. Mission parameters for the first team are presented in Table 1 and the following linear relationship is used:

$$\tau_{c}(X_{i}^{\mu}) = \gamma \times \max(\tau_{a}(X_{i}^{\mu}), \tau_{g}(X_{i,1}^{\mu}, X_{i,n,+2}^{\mu})), \quad \gamma \ge 0, \quad (18)$$

where γ is the recharge ratio. Under (18), the time required to fully recharge the UAV after flying for $\max(\tau_a(X_i^\mu), \tau_g(X_{i,1}^\mu, X_{i,n_\mu+2}^\mu))$ equals $\gamma \times \max(\tau_a(X_i^\mu), \tau_g(X_{i,1}^\mu, X_{i,n_\mu+2}^\mu))$. Hence, $\gamma = 0$ approximates a battery swap system, whereas a larger γ models a slower recharging mechanism.

Table 1: System Parameters Used in the Simulations

Parameter	Value	Parameter	Value
UGV Speed	2.5 m/s	UAV Speed	H: 10 m/s, V: 2 m/s
$\overline{\tau_a}$ (Max flight time)	600 s	γ (Recharge Ratio)	1

4.1. Scalability of the Proposed Algorithm

The performance of the Alg. 1 was evaluated for $n \in \{25, 50, 75, 100\}$ and $m \in \{1, 2, 3, 4, 7, 10\}$. For each team, parameters in Table 1 are used, and each team's initial and final positions are given in Table 2. Results can be seen in Table 3. Computation time of Alg.1 increases with n as expected from its $O(mn + n^3)$ complexity (see Theorem 1). Importantly, in cases where n >> m, the worst-case complexity is dominated by $O(n^3)$ and effectively scales independently of the number of robot teams, m. Overall mission time decreases with increasing number of teams, as teams operate in parallel. The results emphasize the algorithm's ability to handle a wide range of problem sizes and team configurations.

Table 2: Initial (p_0^{μ}) and Final (p_f^{μ}) Positions for All Teams (m = 10)

μ	$p_{\mathbf{o}}^{\mu}$	$p_{ m f}^{\mu}$	μ	$p_{ m o}^{\mu}$	$p_{ m f}^{\mu}$
1	(0, 0, 0)	(1900, 1900, 0)	6	(4000, 2000, 0)	(2200, 2000, 0)
2	(4000, 0, 0)	(2100, 1900, 0)	7	(2000, 4000, 0)	(2000, 2200, 0)
3	(0, 4000, 0)	(1900, 2100, 0)	8	(0, 2000, 0)	(1800, 2000, 0)
4	(4000, 4000, 0)	(2100, 2100, 0)	9	(1000, 0, 0)	(1850, 1950, 0)
5	(2000, 0, 0)	(2000, 1800, 0)	10	(3000, 0, 0)	(2150, 1950, 0)

Table 3: Computation Time and Overall Mission Time (Maximum of the Team Times), $\max_{\mu} \tau(X^{\mu})$, under Alg. 1 for Different Numbers of Robot Teams (*m*) and Problem Sizes (*n*).

	m = 1		m=2				
n	Comp. Time (s)	$\max_{\mu} \tau(X^{\mu})$ (s)	n	Comp. Time (s)	$\max_{\mu} \tau(X^{\mu})$ (s)		
25	0.08 ± 0.02	5000 ± 580	25	0.06 ± 0.01	3870 ± 730		
50	0.22 ± 0.05	6190 ± 640	50	0.13 ± 0.02	4000 ± 510		
75	0.46 ± 0.09	7300 ± 570	75	0.24 ± 0.03	4600 ± 370		
100	0.90 ± 0.20	7900 ± 440	100	0.39 ± 0.05	4800 ± 440		
	m = 3			m = 4			
n	Comp. Time (s)	$\max_{\mu} \tau(X^{\mu})$ (s)	n	Comp. Time (s)	$\max_{\mu} \tau(X^{\mu})$ (s)		
25	0.08 ± 0.01	2530 ± 590	25	0.11 ± 0.01	1580 ± 200		
50	0.11 ± 0.01	2800 ± 500	50	0.10 ± 0.01	1830 ± 110		
75	0.18 ± 0.02	3150 ± 430	75	0.14 ± 0.01	1940 ± 170		
100	0.28 ± 0.03	3460 ± 390	100	0.21 ± 0.02	2100 ± 230		
	m = 7		m = 10				
n	Comp. Time (s)	$\max_{\mu} \tau(X^{\mu})$ (s)	n	Comp. Time (s)	$\max_{\mu} \tau(X^{\mu})$ (s)		
25	0.22 ± 0.04	1460 ± 140	25	0.25 ± 0.05	1420 ± 200		
50	0.26 ± 0.09	1450 ± 140	50	0.34 ± 0.10	1440 ± 150		
75	0.28 ± 0.09	1600 ± 100	75	0.39 ± 0.11	1580 ± 90		
100	0.34 ± 0.11	1660 ± 80	100	0.41 ± 0.12	1620 ± 70		

4.2. Comparison to Branch and Cut

Table 4 presents a comparison between the Branch and Cut, returning global optimum for (3), and Alg.1 for different n. Since Branch and Cut is tractable only for very small n, it cannot be meaningfully applied to multi-team scenarios; therefore, we use m=1, $p_0^1=(0,0,0)$, and $p_1^1=(4000,4000,0)$; and report overall mission time of the single team, $\tau(X^1)$. Branch and Cut computation time grows rapidly with n, as (3) is NP-hard and its complexity scales exponentially. In contrast, Alg.1 yields competitive solutions (observed to get closer to the optimal as n increases) while exhibiting significantly lower computation times, as shown in Table 4.

Table 4: Comparing Computation Time and Overall Mission Time, $\tau(X^1)$, Between Branch and Cut and Alg. 1 for Different Problem Sizes, n.

72	Branch ar	nd Cut	Alg. 1				
n	Comp. Time (s)	$\tau(X^1)$ (s)	Comp. Time (s)	$\tau(X^1)$ (s)			
2	0.05 ± 0.04	1860 ± 410	0.02 ± 0.01	2860 ± 630			
3	0.22 ± 0.27	2190 ± 800	0.03 ± 0.00	2910 ± 590			
4	1.6 ± 4.9	3040 ± 1100	0.03 ± 0.00	3250 ± 680			
5	4.9 ± 7.8	3320 ± 860	0.03 ± 0.00	3320 ± 660			

4.3. Comparison to Metaheuristics

We compared two different metaheuristics, GA and SA, with our method on 5 randomly generated \mathcal{P}_{UAV} (n=15). As with Branch and Cut, the metaheuristics are evaluated in m=1, $p_o^1=(0,0,0)$, and $p_f^1=(4000,4000,0)$ setting, since larger n required for meaningful multi-team cases are not computationally tractable with GA and SA. Note that GA and SA are stochastic algorithms, and their performance varies across runs; therefore, we repeated each instance 3 times and reported averages with the observed variations (\pm corresponds to min-max range in this setting). In contrast, Alg.1 is deterministic, and yields the same result for the same input. Alg.1's performance for this setting is: $\tau(X^1)=4890\pm590~s$, and a computation time of $0.05\pm0.02~s$.

4.3.1. Comparison to Simulated Annealing

The performance of SA depends on temperature control and the cooling schedule, which requires tuning (i.e., setting $T_{\rm max}$, $T_{\rm min}$, and steps) [21]. We used a logarithmic cooling schedule as it provides a balance between exploration and exploitation[22]. The initial feasible solutions had $\tau(X^1) = 15700 \pm 1690$ s, and for all runs we used $T_{\rm min} = 0.01$. The results are shown in Table 5. As expected, increasing the number of steps increases the computational cost, and in most cases improve the solution. However, improvements tend to plateau beyond certain settings. Alg.1 significantly outperforms SA both in computation time and mission time, $\tau(X^1)$. This can be attributed to the fact that, unlike generic metaheuristics, Alg.1 is tailored to exploit the underlying structure of (3).

Table 5: Simulated Annealing Average Computation Time and Overall Mission Time, $\tau(X^1)$, for Different T_{\max} and Number of Steps

	(Comp. Time (s)		$\tau(X^1)$ (s)						
$T_{\rm max}$		Steps		Steps						
	50k	100k	150k	50k	100k	150k				
500	45.66 ± 0.67	84.8 ± 1.2	123.2 ± 1.9	11750 ± 1120	9770 ± 540	9350 ± 620				
1000	45.61 ± 0.68	85.5 ± 1.1	124.6 ± 1.4	12030 ± 1080	9970 ± 700	9410 ± 880				
1500	45.94 ± 0.68	86.21 ± 0.88	124.9 ± 1.2	12160 ± 1000	9980 ± 1140	9850 ± 1150				

4.3.2. Comparison to Genetic Algorithm

The performance of GA is also sensitive to parameter tuning such as mutation rate, mating strategy, selection method and population size [23]. We used steady-state selection, which replaces a portion of the population at each generation to promote gradual convergence [24]. The initial feasible generations had $\tau(X^1) = 10540 \pm 1170s$, and we used a population size of 500 with 50 mating parents in all runs. Results are summarized in Table 6. As expected, more generations yield lower $\tau(X^1)$, but increased computation time. Mutation rate also affected performance, moderate rates gave strong results. Again, Alg.1 consistently outperforms GA.

Table 6: Genetic Algorithm Average Computation Time and Overall Mission Time, $\tau(X^1)$ for Different Mutation Rates and Generations

Mut Rate (%)		Comp. Time (s)		$\tau(X^1)$ (s)					
		Generations		Generations					
	100	150	200	100	150	200			
10	89.45 ± 0.55	133.37 ± 0.87	178.5 ± 1.3	8000 ± 650	7930 ± 840	7610 ± 700			
25	89.78 ± 0.69	133.88 ± 0.87	178.6 ± 1.5	7900 ± 590	7850 ± 570	7550 ± 570			
50	89.66 ± 0.83	133.9 ± 1.2	178.2 ± 1.2	8080 ± 890	8000 ± 790	7660 ± 630			

4.4. Comparison to the State-of-the-Art

We compared our approach to three heuristics [10, 11, 12] that investigate similar energy-aware UAV-UGV planning problems. A fundamental difference of our method and these works is that [10, 11, 12] explicitly assume a single UAV-UGV team, and cannot generalize into multi-team scenarios (m > 1), whereas Alg. 1 can accommodate multi-teams; therefore, these baselines are evaluated only under single-team configuration, m = 1. Another significant difference is the notion of robustness. In [10, 11, 12], the map is assumed to be known a priori. Consequently, those methods are prone to infeasibility in the presence of uncertainty (unknown obstacles, etc.) and

may require complete mission re-planning. In contrast, Alg.1 maintains feasibility without needing a major revision to the plan (Theorem 2). Noting these fundamental differences, we focus on comparing the algorithms based on their efficiency (resulting overall mission time, $\tau(X^1)$ for m=1) and computation time. Since[10, 11, 12] do not consider obstacles, all methods are tested on an obstacle-free map, using VTOL and charging model in (18). We use the parameters in Table 1 with $\gamma \in \{0,1,2\}$ and $p_f^1 = p_o^1 = (0,0,0)$ (since [10, 11, 12] cannot set $p_o \neq p_f$). TSPs and GTSPs are solved using [17] and [18], respectively.

4.4.1. Comparison to [10]

In [10], the authors propose an algorithm, TERRA, to plan for a UAV-UGV team in a monitoring mission using charging stops (rendezvous points). TERRA has five stages: (1) Voronoi tessellations assign monitoring points (\mathcal{P}_{UAV}) to charging stops; (2) a greedy hitting set algorithm refines these assignments; (3) charging stop locations are refined with a Gravitational Optimization Algorithm; (4) a TSP is solved for the UGV path; and (5) a modified A* algorithm computes the path of energyconstrained UAV. Main limitations of the TERRA are: the UGV must remain stationary at charging stops while the UAV visits monitoring points, which can severely slow missions when monitoring points are far apart. Moreover, there is no takeoff/landing modeling and no charging model for UAV, as instantaneous are swaps assumed, which might be impractical in real-world deployment due to the need to carry high number of batteries.

Fig.4 shows that Alg.1 consistently outperforms TERRA in terms of $\tau(X^1)$ across all γ . As n increases, the gap becomes more significant, even with $\gamma = 0$, (as assumed in TERRA).

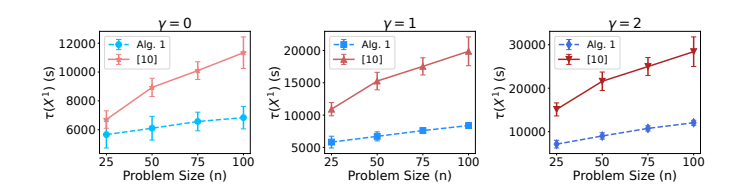


Figure 4: Comparing overall mission time $(\tau(X^1))$ of Alg.1 and TERRA [10] for different problem sizes (n) and recharge ratio (γ) .

As Fig. 5 shows, Alg. 1 consistently achieves lower runtimes, the difference becomes more significant as n increases, emphasizing Alg. 1's scalability.

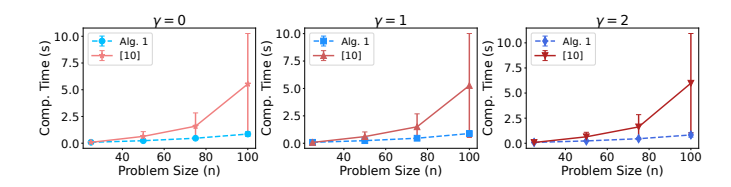


Figure 5: Comparing computation time of Alg.1 and TERRA [10] for different problem sizes (n) and recharge ratio (γ).

4.4.2. Comparison to [12]

In [12], the authors propose a heuristic for UAV-UGV route planning with energy constraints, where UGV operates in a road network. Main limitation of [12] is the road network, restricting UGV to predefined paths (e.g., square grid) and requires UAV monitoring points to be sufficiently close to this roads. Additionally, the method does not model charging. It first solves a TSP to generate the UAV path, and if the energy constraints are violated, a repair algorithm modifies the path (inserts charging stops from a set of predefined charging sites). Alg.1 can operate under mobility constraints, including being constrained to a pre-defined road network. In our comparison, we constrained the UGV to a square road network (an example case in [12]) with edges of 2.5 km, discretized at 10 m resolution when running Alg.1. Fig.6 shows that even under this restriction (i.e., the use of road network, which naturally aligns with the setup of [12]), Alg.1 achieves significantly lower $\tau(X^1)$ when $\gamma = 1, 2$. Moreover, Fig. 7 shows that Alg.1 maintains competitive computational performance.

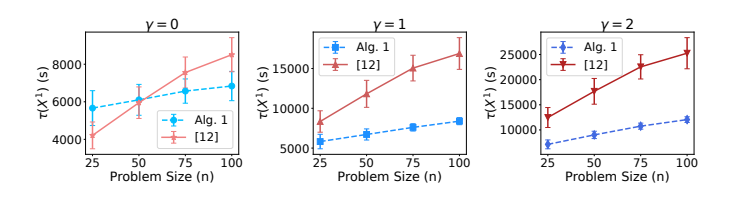


Figure 6: Comparing overall mission time $(\tau(X^1))$ of Alg.1 and the method in [12] for different problem sizes (n) and recharge ratios (γ) .

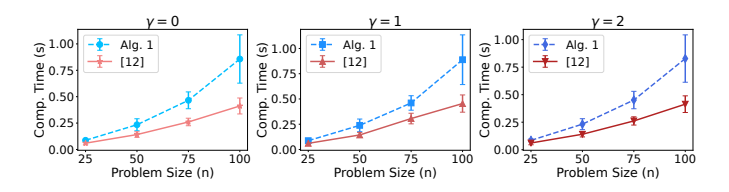


Figure 7: Comparing computation time of Alg.1 and the method in [12] for different problem sizes (n) and recharge ratios (γ) .

4.4.3. Comparison to [11]

In [11], the authors solve a GTSP where nodes represent UAV monitoring points (\mathcal{P}_{UAV}) at discrete battery levels, and edges model transitions. They define two edge types for direct UAV flights with battery depletion, and for UAV recharging while transported by the UGV. Main limitation of this approach is the battery discretization, which effectively limits the consecutive monitoring points the UAV can visit in each tour. We used 10 battery levels for their algorithm to mitigate this limitation while keeping the problem tractable. In [11], the UGV is expected to rendezvous with the UAV at a possibly different location at the end of each flight. Accordingly, the UAV needs to hover at the rendezvous location if it arrives earlier than the UGV. This behavior might cause energy constraint violation, i.e., battery depletion while hovering if the UGV does not arrive at the rendezvous location on time. Our approach avoids

this problem with constraints (3c) and (3d), even in the face of uncertainty.

For evaluation, we tested various UGV speeds (10, 5, and $2.5 \, m/s$), problem sizes (n), and recharge ratios (γ). Results are shown in Table 7 (only averages of successful runs are reported). Based on these, [11] shows high energy constraint violation with low UGV speeds, failing up to 100% of the missions at $2.5 \, m/s$ for some instances. In terms of $\tau(X^1)$, Alg.1 generally matches the performance of the method in [11] and outperforms it in some cases. This is largely because [11] uses discrete battery levels, and forces the UAV to takeoff/land frequently, causing additional delays. Moreover, Alg.1 has significantly lower computation times, as [11] suffers combinatorial growth caused by battery levels.

5. Experiments

Experiments were performed with a team of Crazyflie 2.1 (UAV) and Turtlebot4 (UGV) to demonstrate the applicability our approach. The UAV was constrained to stay on the UGV for a fixed time after each tour, emulating battery swap time. Duration of each tour was constrained to mimic the effect of maximum flight time ($\overline{\tau_a}$). An OptiTrack motion capture (mo-cap) system was used, covering a volume of $6m \times 6m \times 3m$. The software architecture was built on ROS2. Mo-cap streamed realtime pose data for both robots. The UGV navigated with mocap localization. The UAV was controlled via commands for takeoff, land, and navigate \mathcal{P}_{UAV} . A Kalman filter handled state estimation, and a Mellinger controller managed flight control.

The scenario illustrated in Fig.8 had 15 points in \mathcal{P}_{UAV} . Alg.1 was used to generate a plan X without any knowledge of the obstacles. The plan had three tours as shown in Fig.8a. As the team followed this plan, if a release/collect point was occupied by an obstacle, an alternative was selected within a radius of $(\hat{\sigma}_a^{\mu,i}(X) \times v_H^{\text{avg}})/2$ of the original point while ensuring the distance between the respective release and collect points did not increase by more than $\hat{\sigma}_g^{\mu,i}(X) \times v_g^{\text{avg}}$. This maintained feasibility under the UAV's energy limitation (see Corollary 1 and Remark 1). A new release point was selected for the second tour during the mission due to an unknown obstacle as shown in Fig. 8b. Experiment video can be found in supplementary materials, and is available online.⁵

6. Conclusion

We presented RSPECT, a scalable and efficient heuristic algorithm for robust planning of energy-constrained UAVs and mobile charging stations (UGVs) to perform long-horizon aerial monitoring missions. We provided theoretical results on the complexity and robustness of our approach. These theoretical results were also supported by simulations that demonstrated the performance of our approach and compared it to some standard optimization techniques as well as other related

⁵Video link: https://youtu.be/QN6FRDtdvd4

Table 7: Evaluating Computation Time, Energy Constraint Violation, and Overall Mission Time, $\tau(X^1)$, with different UGV speeds, problem sizes (n) , and recharge	
ratios (γ). Left: Alg. 1. Right: Method in [11].	

	(1), =																		
UGV Speed			Alg. 1								Method in [11]								
OG v Speed	"		Comp. Time (s)	Ener	Inergy Const. Violation $\tau(X^1)$			$\tau(X^1)$ (s)			Energy	Const. V	Violation	$\tau(X^1)$ (s)				
		γ=0	γ=1	γ=2	γ=0	γ=1	γ=2	γ=0	γ=1	γ=2	γ=0	γ=1	γ=2	γ=0	γ=1	γ=2	γ=0	γ=1	γ=2
	25	0.08 ± 0.02	0.08 ± 0.02	0.08 ± 0.02	0%	0%	0%	5660 ± 930	5820 ± 910	7130 ± 880	-	-	-	100%	100%	100%	-	-	-
2.5	50	0.21 ± 0.04	0.22 ± 0.05	0.220 ± 0.04	0%	0%	0%	6100 ± 820	6710 ± 700	9010 ± 730	-	-	2.76 ± 0.16	100%	100%	64%	-	-	9470 ± 390
2.3	75	0.48 ± 0.08	0.46 ± 0.09	0.46 ± 0.07	0%	0%	0%	6570 ± 650	7600 ± 460	10750 ± 600	-	7.45 ± 0.73	7.56 ± 0.84	100%	88%	40%	-	9160 ± 370	13040 ± 250
	100	0.86 ± 0.18	0.90 ± 0.23	0.84 ± 0.17	0%	0%	0%	6840 ± 780	8380 ± 440	12050 ± 570	-	14.4 ± 1.4	17.6 ± 2.3	100%	72%	16%	-	11770 ± 330	16130 ± 400
	25	0.06 ± 0.01	0.07 ± 0.01	0.06 ± 0.01	0%	0%	0%	2840 ± 290	3790 ± 350	5380 ± 500	0.52 ± 0.05	0.51 ± 0.05	0.50 ± 0.08	80%	8%	0%	2710 ± 230	3790 ± 250	4440 ± 290
5.0	50	0.20 ± 0.03	0.210 ± 0.03	0.21 ± 0.04	0%	0%	0%	3470 ± 270	5190 ± 290	7530 ± 460	2.69 ± 0.38	2.48 ± 0.30	2.93 ± 0.39	44%	0%	0%	3630 ± 190	5470 ± 190	7130 ± 160
3.0	75	0.45 ± 0.08	0.45 ± 0.08	0.45 ± 0.08	0%	0%	0%	3910 ± 140	6210 ± 150	9040 ± 200	6.84 ± 0.82	6.89 ± 0.59	9.90 ± 2.0	28%	0%	0%	4250 ± 140	7490 ± 170	9940 ± 120
	100	0.82 ± 0.16	0.83 ± 0.16	0.83 ± 0.17	0%	0%	0%	4350 ± 190	7150 ± 350	10490 ± 570	14.5 ± 2.2	15.4 ± 2.4	18.2 ± 1.5	4%	0%	0%	5000 ± 200	9450 ± 200	12770 ± 150
	25	0.06 ± 0.01	0.06 ± 0.01	0.06 ± 0.01	0%	0%	0%	2270 ± 190	3570 ± 370	5110 ± 580	0.48 ± 0.04	0.48 ± 0.04	0.54 ± 0.06	0%	0%	0%	2230 ± 130	2910 ± 150	3490 ± 110
10.0	50	0.21 ± 0.06	0.20 ± 0.036	0.20 ± 0.03	0%	0%	0%	2970 ± 130	4940 ± 170	7200 ± 200	2.23 ± 0.20	2.53 ± 0.27	2.72 ± 0.28	0%	0%	0%	3000 ± 110	4780 ± 85	6280 ± 72
10.0	75	0.48 ± 0.20	0.45 ± 0.07	0.44 ± 0.08	0%	0%	0%	3517 ± 86	6144 ± 92	9010 ± 110	5.8 ± 0.6	7.6 ± 1.2	7.8 ± 0.6	0%	0%	0%	3670 ± 92	6830 ± 62	9150 ± 47
	100	0.88 + 0.38	0.82 ± 0.16	0.83 ± 0.17	0%	0%	0%	3970 + 160	7050 + 350	10390 + 570	13.9 + 1.5	14.8 + 1.7	23.4 ± 6.0	0%	0%	0%	4270 + 120	8800 + 110	11990 + 81

			UAV ←— 🚱	
				*
START END A Release 1 Collect 1 A Release 2 Collect 2				· ·
Release 3 Collect 3 UGV Path	<u> </u>	UAV - UGV Team	(b)	

Figure 8: (a) Plan generated via Alg.1: the solid lines show the UAV's tours and the dashed lines show the UGV's path (gray when transporting the UAV). (b) Snapshot from the second tour: upward triangle is the planned release point, star is the modified release point, downward triangle is the collect point.

works ([10, 11, 12]). Experiments were also provided for validation.

Future work includes adapting our approach to other long-horizon missions such as patrolling, SLAM, search, and exploration with UAV-UGV teams. Moreover, we plan to enhance our approach with more on-board autonomy (e.g., for energy monitoring/harvesting, reactive planning and coordination, dynamic environment/obstacles). Finally, we plan to incorporate learning-based approaches for improving the overall performance in stochastic scenarios.

References

- [1] P. Tokekar, J. Vander Hook, D. Mulla, V. Isler, Sensor planning for a symbiotic uav and ugv system for precision agriculture, IEEE transactions on robotics 32 (6) (2016) 1498–1511.
- [2] S. M. et al., On the use of unmanned aerial systems for environmental monitoring, Remote Sensing 10 (2018) 641. doi:10.3390/rs10040641.
- [3] Y. Ham, et al., Visual monitoring of civil infrastructure systems via camera-equipped unmanned aerial vehicles (uavs): a review of related works, Visualization in Engineering 4 (12 2016). doi:10.1186/s40327-015-0029-z.
- [4] H. Ren, Y. Zhao, W. Xiao, Z. Hu, A review of uav monitoring in mining areas: current status and future perspectives, International Journal of Coal Science & Technology 6 (08 2019). doi:10.1007/s40789-019-00264-5.

- [5] P. B. et al., Uav deployment exercise for mapping purposes: Evaluation of emergency response applications, Sensors 15 (7) (2015) 15717–15737.
- [6] A. S. Asarkaya, D. Aksaray, Y. Yazıcıoğlu, Temporallogic-constrained hybrid reinforcement learning to perform optimal aerial monitoring with delivery drones, in: Proc. IEEE ICUAS 2021, 2021, pp. 285–294.
- [7] Y. Mulgaonkar, V. Kumar, Autonomous charging to enable long-endurance missions for small aerial robots, in: Micro- and Nanotechnology Sensors, Systems, and Applications VI, Vol. 9083, 2014, p. 90831S. doi:10.1117/12.2051111.
 - URL https://doi.org/10.1117/12.2051111
- [8] S. S. Bacanli, E. Elgeldawi, D. Turgut, Charging station placement in unmanned aerial vehicle aided opportunistic networks, in: IEEE International Conference on Communications, 2021, pp. 1–5. doi:10.1109/ICC42927. 2021.9500848.
- [9] N. Nigam, et. al., Control of multiple uavs for persistent surveillance: Algorithm and flight test results, IEEE Transactions on Control Systems Technology 20 (2012) 1236–1251. doi:10.1109/TCST.2011.2167331.
- [10] F. Ropero, P. Muñoz, M. D. R-Moreno, Terra: A path planning algorithm for cooperative ugv-uav exploration, Engineering Applications of Artificial Intelligence 78 (2019) 260-272. doi:https://doi.org/10.1016/j.engappai.2018.11.008. URL https://www.sciencedirect.com/science/article/pii/S095219761830246X
- [11] K. Yu, A. K. Budhiraja, P. Tokekar, Algorithms for routing of unmanned aerial vehicles with mobile recharging stations, in: 2018 IEEE International Conference on Robotics and Automation (ICRA), 2018, pp. 5720–5725. doi:10.1109/ICRA.2018.8460819.
- [12] P. Maini, K. Sundar, M. Singh, S. Rathinam, P. B. Sujit, Cooperative aerial—ground vehicle route planning with fuel constraints for coverage applications, IEEE Transactions on Aerospace and Electronic Systems 55 (6) (2019) 3016–3028. doi:10.1109/TAES.2019.2917578.

- [13] S. Seyedi, Y. Yazicioğlu, D. Aksaray, Persistent surveillance with energy-constrained uavs and mobile charging stations, IFAC-PapersOnLine 52 (20) (2019) 193–198. doi:10.1016/j.ifacol.2019.12.157.
- [14] G. Shi, et.al, Risk-aware uav-ugv rendezvous with chance-constrained markov decision process (2022). arXiv:2204.04767. URL https://arxiv.org/abs/2204.04767
- [15] X. Lin, Y. Yazıcıoğlu, D. Aksaray, Robust planning for persistent surveillance with energy-constrained uavs and mobile charging stations, IEEE Robotics and Automation Letters 7 (2) (2022) 4157–4164. doi:10.1109/LRA. 2022.3146938.
- [16] J. E. Mitchell, Branch-and-cut algorithms for combinatorial optimization problems, Handbook of applied optimization 1 (1) (2002) 65–77.
- [17] N. Christofides, Worst-case analysis of a new heuristic for the travelling salesman problem, Operations Research Forum 3 (1) (2022) 20.
- [18] S. L. Smith, F. Imeson, GLNS: An effective large neighborhood search heuristic for the generalized traveling salesman problem, Computers & Operations Research 87 (2017) 1–19.
- [19] Y. Ye, E. Tse, An extension of karmarkar's projective algorithm for convex quadratic programming, Mathematical Programming 44 (1-3) (1989) 157–179.
- [20] Y. Guo, et. al., Precision landing test and simulation of the agricultural uav on apron, Sensors 20 (12) (2020). doi:10.3390/s20123369. URL https://www.mdpi.com/1424-8220/20/12/ 3369
- [21] E. Aarts, J. Korst, W. Michiels, Simulated annealing, in: E. K. Burke, G. Kendall (Eds.), Search Methodologies: Introductory Tutorials in Optimization and Decision Support Techniques, Springer US, Boston, MA, 2005, pp. 187–210. doi:10.1007/0-387-28356-0_7. URL https://doi.org/10.1007/0-387-28356-0_7
- [22] Y. Nourani, B. Andresen, A comparison of simulated annealing cooling strategies, Journal of Physics A: Mathematical and General 31 (41) (1998) 8373. doi:10.1088/0305-4470/31/41/011. URL https://dx.doi.org/10.1088/0305-4470/31/41/011
- [23] M. Gen, R. Cheng, Genetic algorithms and engineering optimization, John Wiley & Sons, 1999.
- [24] J. Smith, On replacement strategies in steady state evolutionary algorithms, Evolutionary Computation 15 (1) (2007) 29-59. arXiv:https://direct.mit.edu/evco/article-pdf/15/1/29/1493717/evco.2007. 15.1.29.pdf, doi:10.1162/evco.2007.15.1.29.

URL https://doi.org/10.1162/evco.2007.15.1. 29